



28-Gbps interconnect based on a plastic optical engine providing reduced modal dispersion

Yong-Geon Lee^{a,b}, Yung-Sung Son^a, Sang-Shin Lee^{b,*}

^a Optomind Inc., Suwon 16690, South Korea

^b Department of Electronic Engineering, Kwangwoon University, 20 Kwangwoon-ro, Nowon-gu, Seoul 01897, South Korea

ARTICLE INFO

Keywords:

Optical interconnect
Active optical cable
Optical engine
Plastic beam coupler
Modal dispersion
Vertical cavity surface emitting laser

ABSTRACT

A plastic optical engine that reduces modal dispersion was proposed and implemented for a 28-Gbps interconnect; its dependence on the angular distribution of the focused beam for a transmitter was examined. The beam coupler was designed using two focused beam numerical apertures (FNAs) for transmitter. The modal dispersion of the smaller FNA was superior to the larger FNA by 6.2 ps at the backshell temperature of 75 °C for a 150-m OM3 fiber. The manufactured optical engine with smaller FNA supported effective fiber bandwidth for error-free data transmission over a 150-m-long OM3 fiber at 28 Gbps. Decreasing the FNA suppresses modal dispersion, thus enabling the use of longer OM3 fibers.

1. Introduction

The advent of cloud computing and a variety of web applications has driven the demand for large-capacity warehouse-scale data centers. Data centers have emerged as an indispensable infrastructure for empowering the ever-growing data capacity. Warehouse-scale data centers comprise hundreds of thousands of servers, which communicate with each other via interconnection networks featuring high performance and low latency [1–5]. Recently, modernized data centers have been developed to understand the topology of commodity ethernet switches [6]. Network architects for an intra-data center have adopted a structure based on a top-of-rack switch, exhibiting compactness and high density [7]. For the link between the server and the top-of-rack switch, either electrical copper or optical connection can be used depending on the link length. Optical fiber-based transmission is one of the most conspicuous technologies for building data centers owing to its high bandwidth, small size, light weight, and low power consumption feature [1]. To that end, a multimode fiber (MMF) in combination with a vertical cavity surface emitting laser (VCSEL) is typically used to embody a short-reach interconnect [8–10]. Especially, the interconnect such as an active optical cable (AOC), which resorts to a VCSEL at 850-nm wavelength in tandem with an MMF rather than a single mode fiber (SMF), is regarded as one of the most prominent candidates to act as a short-reach link. The MMF is preferred over the SMF for realizing data communications in a short-reach network because of its relaxed alignment tolerance. However, the MMF may be disadvantageous due to the excitation of multiple spatial modes that lead to different group velocities, apart from its inhomogeneity and ellipticity. A pulse signal,

which is initially launched in the form of a single spatial mode, may be deformed to excite other spatial modes that travel with different group velocities, thus causing the pulse spreading to limit the data rate. In an attempt to mitigate the problems associated with modal dispersion, numerous schemes were suggested, e.g., an algorithm based on adaptive optics compensating for modal dispersion and convex optimization capitalizing on a spatial light modulator with respect to the amplitude, phase, and polarization [11–14]. For the link, the speed may be limited by the operation speed of the VCSEL, the photodetector (PD), and the driver circuit, as well as the bandwidth of the fiber, while the distance is constrained by the bandwidth and attenuation of the fiber and the coupled power. For such an interconnect, the link is limited to a distance of 100 m for an OM4 MMF and a speed of 28 Gbps. The standard maximum operation distance is currently 70 m for an OM3 MMF. The link distance for high data rates is largely dependent on the characteristics of the laser and the fiber [15,16].

The aim of this work is to resolve the limitation of transmission distance by taking advantage of an optical engine to reduce the group delay and modal dispersion. For the proposed optical engine, the light source is tuned using a dual lens belonging to a beam coupler. The modulated beam is delivered from the transmitter (Tx) to the receiver (Rx) via a glass optical fiber (GOF). The beam coupler, in which the body and cover are integrated with the fiber guide, is simultaneously incorporated into the Tx and the Rx. A pair of precisely controlled reference holes are inscribed in the printed circuit board (PCB), onto which the VCSEL and PD are mounted. The VCSEL-to-GOF and GOF-to-PD couplings are passively mediated by the beam coupler in collaboration with the reference hole. The realized optical engine, serving as an AOC

* Corresponding author.

E-mail address: slee@kw.ac.kr (S.-S. Lee).

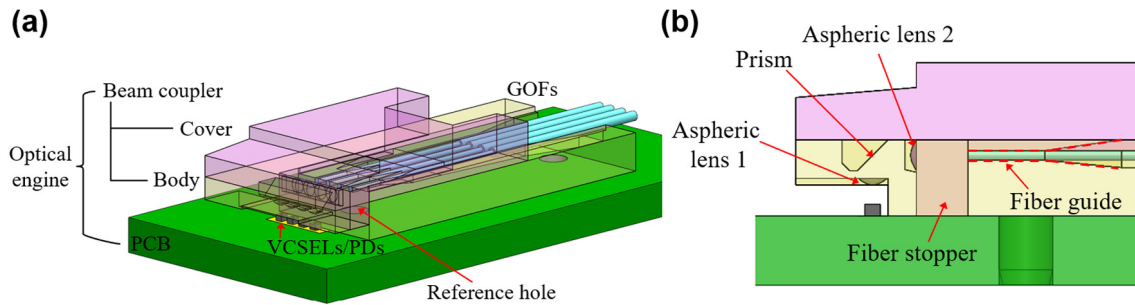


Fig. 1. Proposed optical engine for implementing 28-Gbps interconnect. (a) Configurations of the Tx/Rx optical engine and (b) the beam coupler.

type of short-reach interconnect, allows for a fully passive assembly with the help of a cost-effective precise alignment. Furthermore, the optical engine can readily facilitate volume production based on an advanced plastic injection molding technique [17,18]. For the optical engine associated with the proposed AOC, serving as a short-reach interconnect, Tx is directly linked to Rx via a fiber. Meanwhile, the conventional transceiver engages an optics part based on a fiber optic patch cord, which suffers from Fresnel reflection loss caused by an air gap between the lens and the fiber. Note that the AOC can facilitate a convenient plug-and-play deployment, requiring no additional performance tests for the link.

2. Proposed optical engine and its design

Fig. 1 illustrates a schematic of the proposed Tx/Rx optical engine enabling the 28-Gbps interconnect. The Tx involves a beam coupler connected to a fiber, while a VCSEL, which is mounted on the PCB, acts as an infrared light source. The Rx is similarly constructed by replacing the VCSEL with a PD. The plastic beam coupler consists of aspheric lenses, a right-angle prism, a fiber stopper, and a fiber guide. The beam coupler is designed to play a role of transmitting light either from VCSEL to GOF or from GOF to PD. For the Tx optical engine, an infrared beam emitted by each VCSEL is collimated by aspheric lens 1, which is tethered to the body. The collimated beam passes through the prism via total internal reflection. The reflected beam is focused on the fiber by aspheric lens 2. For the Rx, the beam emanating from the GOF is collimated by aspheric lens 2, then collected by the PD via aspheric lens 1. The optical interconnect is then completed by linking the Tx and Rx optical engine via the GOF.

Since modal dispersion plays an integral role in reliably transmitting high-speed data via the proposed optical engine, we elaborated on the mechanism that causes modal dispersion in terms of group velocity. Modal dispersion for the MMF is attributed to the difference in group velocities of the multiple guided modes. The group velocity/delay is related to the higher-order modes of the coupled beam for the Tx as well as the numerical aperture (NA) of the fiber. The total number of modes is proportional to the NA. The proposed Tx optical engine was designed to primarily support lower-order modes near the fundamental mode by constraining the angular distribution of the focused beam so that modal dispersion can be improved so as to effectively increase the optical fiber bandwidth. However, higher order modes are likely to be excited over the course of sufficiently long propagation due to impurities in the fiber, fiber bending, and degraded characteristics of the VCSEL at elevated temperatures [19]. Consequently, there might be a certain limit to the improvement of modal dispersion.

The dependence of modal dispersion on angular distribution of the focused beam for the Tx was examined through simulations employing a ray-optic tool, LightTools. The VCSEL operating at $\lambda = 850$ nm provides a divergence of 30° in full angle. The GOF has a $50\text{-}\mu\text{m}$ core and an NA of 0.2, while the lens is made of polycarbonate ($n = 1.571$ @ $\lambda = 850$ nm). The angular distribution of the focused beam for the Tx refers to the range over which the intensity drops to $1/e^2$ of the

peak level at the center. Beam couplers I and II share in the same aspheric lens 1, while their focal lengths, which are determined by the aspheric lens 2, are different. As depicted in Fig. 2(a), the focused beam is characterized by the focused beam NA (FNA). The focused beam, which is deemed to decrease with increasing FNA, is calculated to be $26\ \mu\text{m}$ and $22\ \mu\text{m}$ in width for beam couplers I and II, respectively, implying the focused beam is smaller than the core of the fiber. For the Rx, the focused beam size at the PD is $38\ \mu\text{m}$ and $46\ \mu\text{m}$ for beam couplers I and II, respectively.

In Fig. 2(b), θ_{IN} refers to the angle of the ray impinging upon the fiber core, θ_α is the angle between the refracted ray and the fundamental ray, and θ_β is the angle corresponding to the total internal reflection at the core-cladding interface. Note that L_{FM} and L_{IN} represent the propagation distance for the fundamental ray and the obliquely incident ray, respectively. The modal dispersion value is obtained by $\Delta\tau_{NA} = \frac{L_{NA}}{2cn_{clad}} NA^2$ and $\Delta\tau_{FNA} = \frac{L_{FNA}}{2cn_{clad}} FNA^2$ for $\theta_{IN} = \theta_{NA}$ and θ_{FNA} , respectively, by applying the NA of the OM3 fiber and the FNA. Here, c is the speed of light while n_{clad} is the refractive index of cladding. The modal dispersion value decreases with decreasing θ_{IN} , indicating that $\theta_{NA} > \theta_{FNA}$ results in $\Delta\tau_{NA} > \Delta\tau_{FNA}$. The modal dispersion value is expected to be suppressed by reducing the number of guided modes to decrease the FNA [20,21].

As shown in Fig. 3, beam coupler I and beam coupler II exhibit effective angular distributions covering up to 6.8° and 8.4° , respectively, which are translated into the FNAs of 0.118 and 0.146. For the designed beam coupler, modal dispersion for beam coupler I ($\Delta\tau_{BC I}$) is smaller than that for beam coupler II ($\Delta\tau_{BC II}$). Modal dispersion is hence evaluated in terms of jitter in relation to an eye pattern. The FNA can be changed by adjusting the focal length. For instance, when the FNA is designed to be small, the focal length is increased via aspheric lens 2. The fiber stopper is to be correspondingly extended by the focal length. The modal dispersion may improve with smaller FNA to such an extent that the relevant alignment tolerance is not significantly deteriorated.

3. Implementation of the proposed optical engines and their characterization

The proposed optical engine is passively designed via a simplistic pick-and-place scheme, using no expensive aligning machine with sub-micron accuracy. The optical engine incorporates beam couplers manufactured through injection molding in polycarbonate, serving as an optically transparent material. This assembly process is described in Fig. 4. The guide pin protruding from the beam coupler was inserted into the reference hole in the PCB. Both VCSEL and PD were subsequently mounted with the help of the reference hole. The GOF was finally arranged along the groove, which is inscribed in the fiber guide and the stopper.

Considering that the alignment performance of the VCSEL/PD, beam coupler, and GOF largely depends on the quality of elements constituting the optical engine, we explored the tolerance for the VCSEL and PD. The tolerance was estimated by checking the optical power available

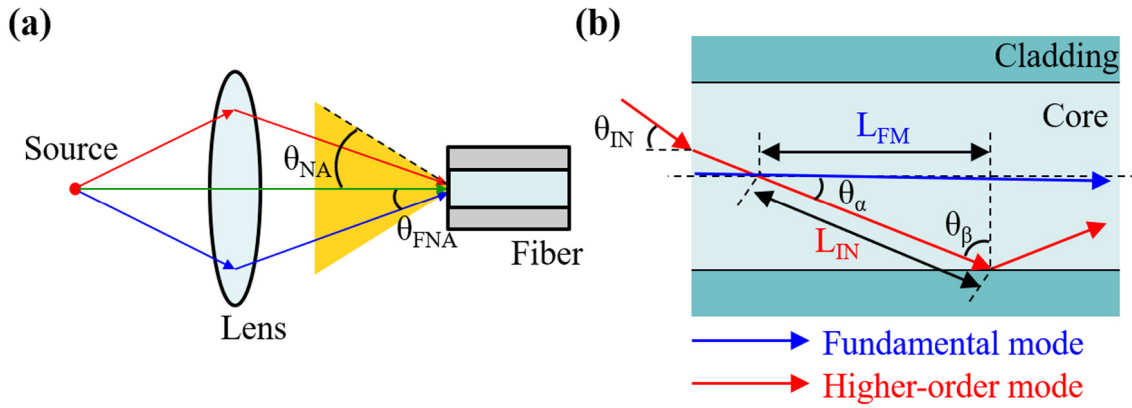


Fig. 2. (a) Description of propagation angles corresponding to the NA and FNA (b) Difference in time of travel for the higher order mode and fundamental mode according to the incident angle θ_{IN} .

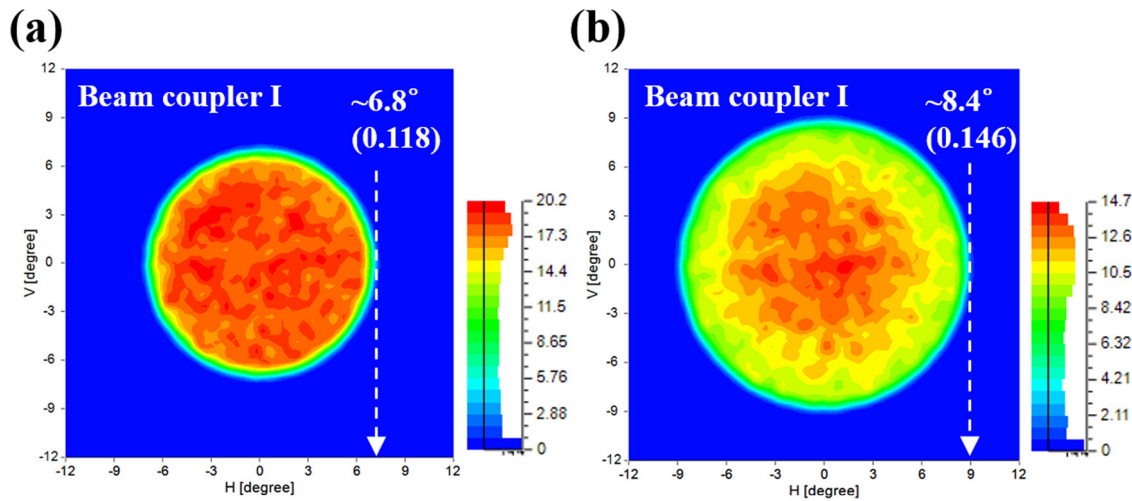


Fig. 3. Angular distribution of the focused beam for the Tx using (a) beam coupler I and (b) beam coupler II.

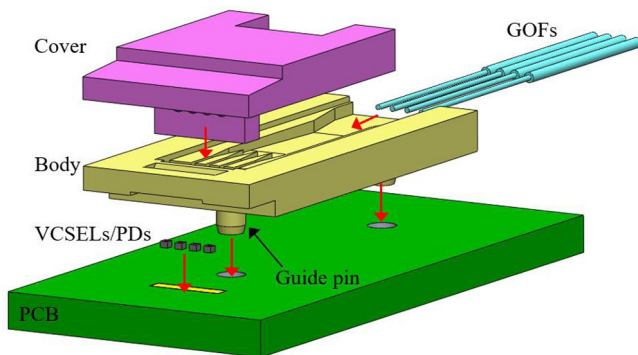


Fig. 4. Assembly procedure for the proposed Tx/Rx optical engine.

from the GOF core of 50- μm diameter and from the PD with an effective aperture of 42 μm in diameter, when the VCSEL and PD were displaced with intervals of 5 μm (Fig. 5). In the case of Tx, the VCSEL-to-GOF coupling for beam coupler I and beam coupler II caused a minimum loss of 0.7 dB. The alignment tolerance with reference to the 3-dB coupling loss was approximately 30 μm and 40 μm along the x and y axes, respectively. In the case of Rx, the calculated PD tolerance was 30 μm and 26 μm along the x and y axes, respectively. The GOF-to-PD coupling was as small as 0.7 dB and 1.0 dB. According to these results,

our optical engine provides a sufficiently large alignment tolerance to facilitate the assembly procedure.

Considering that the misalignment of VCSEL affects the FNA, we explored variations in the angular distribution of the focused beam in terms of the VCSEL displacement for the case of Tx, as depicted in Fig. 6, with reference to the displacement leading to a 3-dB coupling loss. For beam coupler I, the displacement is calculated to be +15 μm for Δx and Δy . The incidence angle increases by about 0.7 $^\circ$ while the FNA is 0.131. For beam coupler II, the corresponding displacement is +20 μm . The angle of incidence increases by about 0.5 $^\circ$ while the FNA is 0.155. Despite the misalignment of the VCSEL, it is guaranteed that the FNA for the beam couplers is below a 0.2 NA for the OM3 fiber. The angular distribution is just slightly affected by the VCSEL displacement.

To explore the coupled power to the fiber with respect to the FNA for the Tx, we examined the encircled flux based on the near-field pattern [22–24]. As shown in Fig. 7, the encircled flux was monitored via a GOF (OM3) of 10-m length. Under an encircled flux of 0.86, the difference in the centroid radius between beam couplers I and II is observed to be 0.9 μm . It has been consequently confirmed the output NA of the fiber crucially hinges on the FNA. As depicted in Fig. 2, the group delay in the time domain between the higher-order modes and the fundamental mode signifies the modal dispersion, which can be extracted from an optical eye jitter. To analyze the impact of FNA on modal dispersion, the proposed optical engine was tested to transmit a $2^{31}-1$ pseudorandom bit sequence (PRBS) signal at 28 Gbps via GOFs (OM3) of 50-m and 150-m lengths. Here, the clock and data recovery function are not used, with beam couplers I and II delivering the same

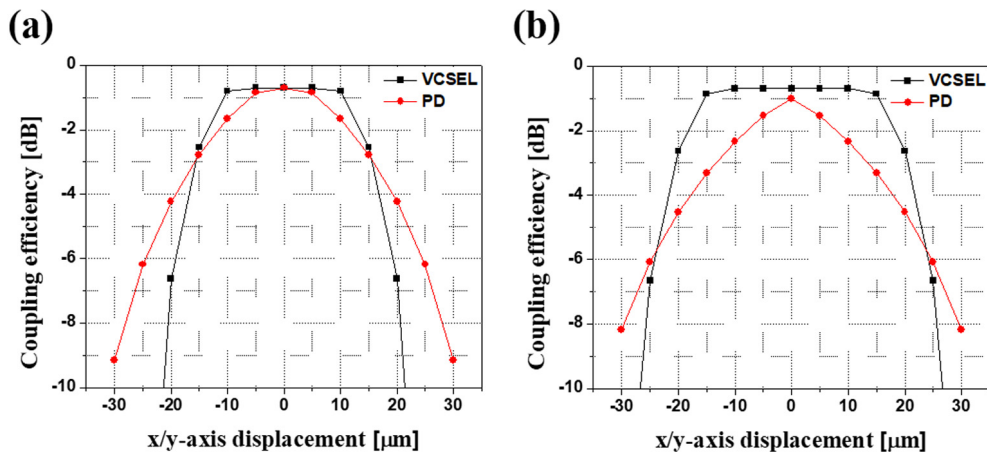


Fig. 5. Calculated coupling efficiency depending on the VCSEL/PD displacement along the x/y axes for the cases of (a) beam coupler I and (b) beam coupler II.

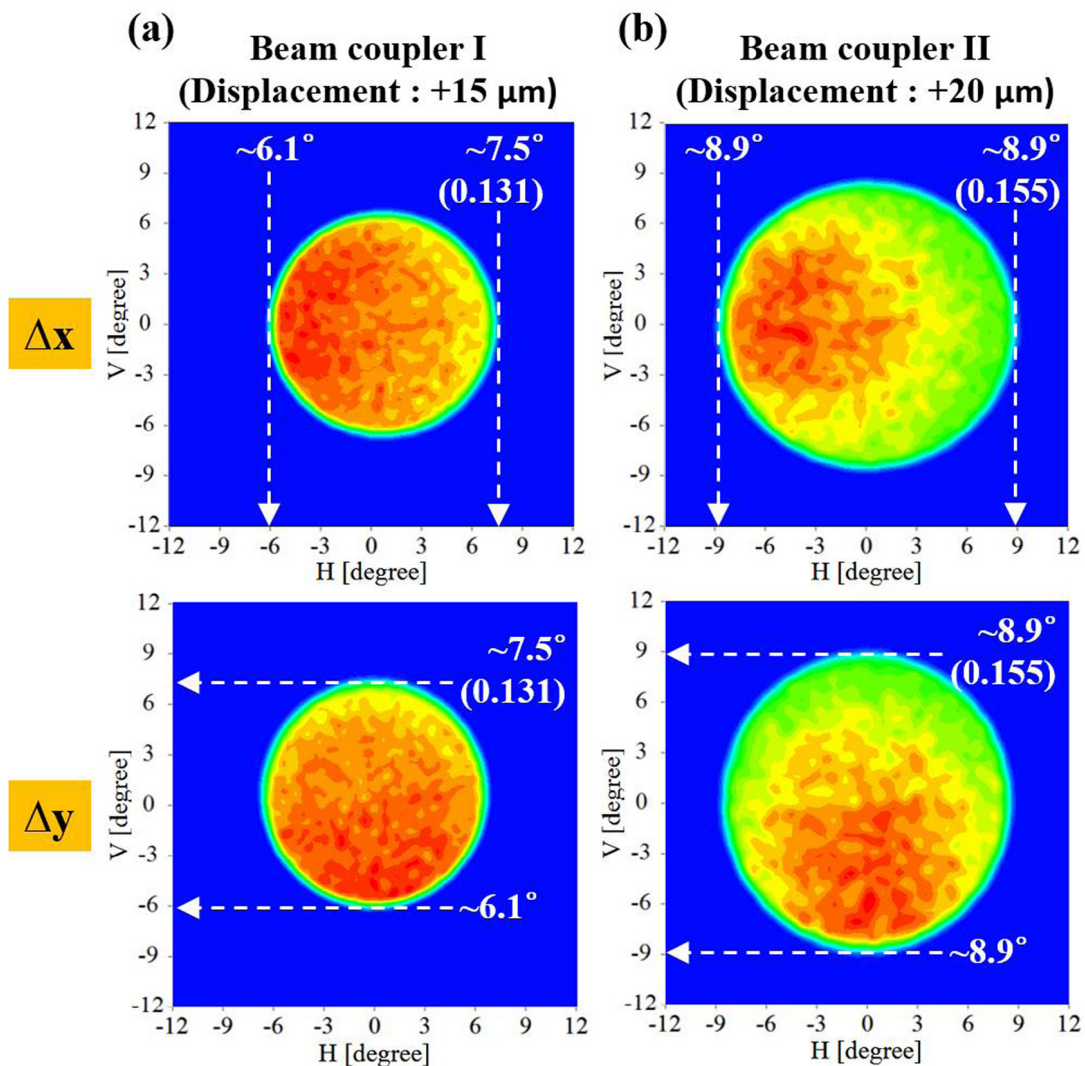


Fig. 6. Variation in the angular distribution of the focused beam for the Tx according to the VCSEL displacement for the cases of (a) beam coupler I and (b) beam coupler II.

optical power. The optical engine with the quad small form-factor pluggable (QSFP) configuration was tethered to the Tx/Rx evaluation board (Fig. 8).

A PPG (Keysight, N4951B) was employed to drive the primary channel to be measured, while a secondary PPG (multiLane, ML4039)

was additionally employed to drive the remaining three channels. To observe an optical eye pattern, the optical signal corresponding to the Tx was transported to a scope (Anritsu MP2110A). The optical signal was obtained in response to an input electrical eye signal, whose peak-to-peak jitter reached 8.2 ps. The influence of the VCSEL misalignment

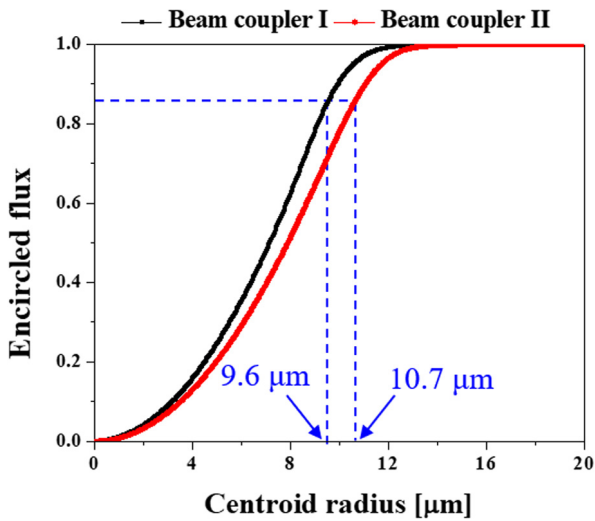


Fig. 7. Measured encircled flux of the designed beam couplers.

was explored for a 50-m long OM3 fiber in the case of beam coupler I as shown in Fig. 9. The modal dispersion corresponding to coupling losses of 1.5 dB and 3 dB was represented by timing jitters of 5 ps and 7 ps, respectively. For beam coupler II, the timing jitter increased by 6.1 ps and 8.3 ps, respectively. Noting the timing jitter exhibits slight variations over the 3-dB coupling loss range for the beam couplers, the proposed optical engine is suitable for a passively-aligned optical engine. It is remarked that beam coupler I is superior to beam coupler II in terms of the timing jitter characteristics.

We investigated the impact of FNA on the modal dispersion. Fig. 10 shows the optical eye patterns for $2^{31}-1$ PRBS signals, depending on the fiber length and the backshell (case) temperature. The peak-to-peak jitter for the input signal was 8.2 ps. For beam coupler I, the observed modal dispersion for the transmitted signal relative to the input signal was 5 ps and 6.9 ps for lengths of 50 m and 150 m, respectively. Likewise, for beam coupler II, the modal dispersion for the 50-m case was 6.1 ps while that for the 150-m case was 9.6 ps, implying that the effect of FNA on the modal dispersion becomes substantial when both the data rate and the transmission length increase. The jitter increased

by 2.7 ps and 4.3 ps for beam couplers I and II for the length of 50 m, respectively, when the backshell temperature increased from 40 °C to 75 °C. The corresponding jitter degradation was 4.5 ps and 8 ps for beam couplers I and II for the length of 150 m, respectively. The modal dispersion can be suppressed by reducing the FNA, thereby enabling the use of longer OM3 fibers. To investigate the effect of FNA, the Tx was evaluated over a transmission distance of 150 m in terms of the bit error rate (BER) in response to $2^{31}-1$ PRBS signals, operating at 28 Gbps, through an error detector (Keysight, N4952A), with the clock and data recovery function activated. The BER was measured for the same Rx incorporating beam coupler I. As shown in Fig. 11, the BER characteristics were monitored in accordance with the optical modulation amplitude of the Tx, which is adjusted by use of a variable optical attenuator whose attenuation ranges from 3 dB to 60 dB. For all the channels, the Tx optical modulation amplitude corresponding to 10^{-12} BER was checked to be -9.1 and -7.8 dBm for beam couplers I and II, respectively, at a temperature of 40 °C. For loop-back samples based on beam couplers I and II, which are tethered to a 150-m long OM3 fiber, an error-free transmission was obtained for all the channels overnight at the same temperature in the absence of the optical attenuator. At 75 °C, beam coupler I and beam coupler II were error-free and below 10^{-11} , respectively. Hence, the proposed optical engine provides an effective fiber bandwidth, enabling a transmission over a 150-m long OM3 fiber at a data rate of 28 Gbps and proposed optical engines incorporating beam couplers I and II can successfully manage a data rate as fast as 28 Gbps, regardless of their modal dispersions.

4. Conclusion

A multi-channel optical engine was developed to efficiently mitigate modal dispersion and enable a 28-Gbps interconnect. Alignment between the beam coupler, VCSEL/PD, and the OM3 fiber was carried out in a passive manner using a pair of reference holes in the PCB. The dependence of modal dispersion on the angular distribution of the focused beam for the Tx was examined by conducting ray-optic simulations. For the 150-m OM3 fiber, modal dispersion for the smaller FNA was smaller than that for the larger FNA by up to 6.2 ps at the backshell temperature of 75 °C. Modal dispersion can be reduced by decreasing the FNA to allow for the use of longer OM3 fibers. For the 150-m long loop-back sample providing the smaller FNA, data transmission based on $2^{31}-1$ PRBS signals was observed to be error-free

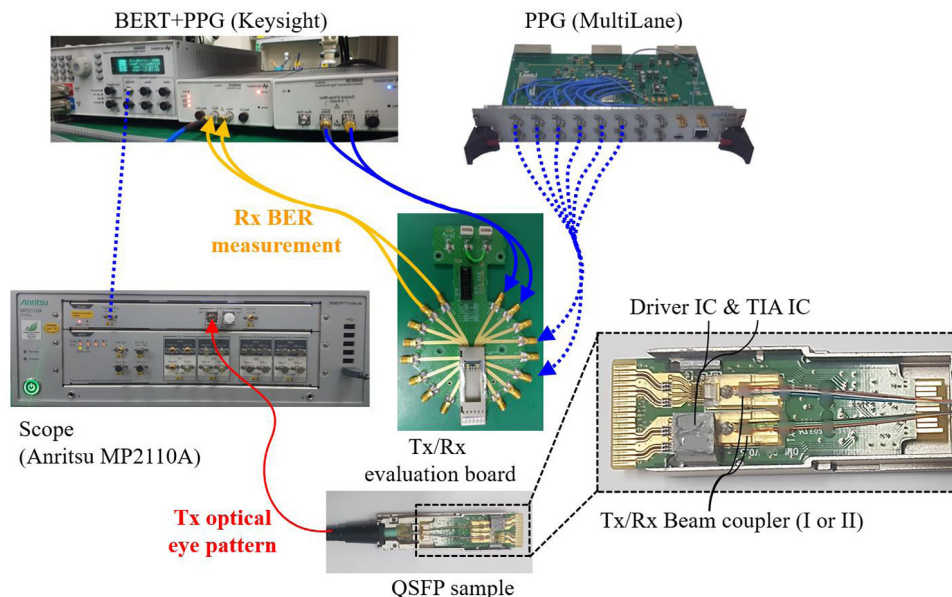


Fig. 8. Experimental setup for characterizing the performance of the proposed optical engine.

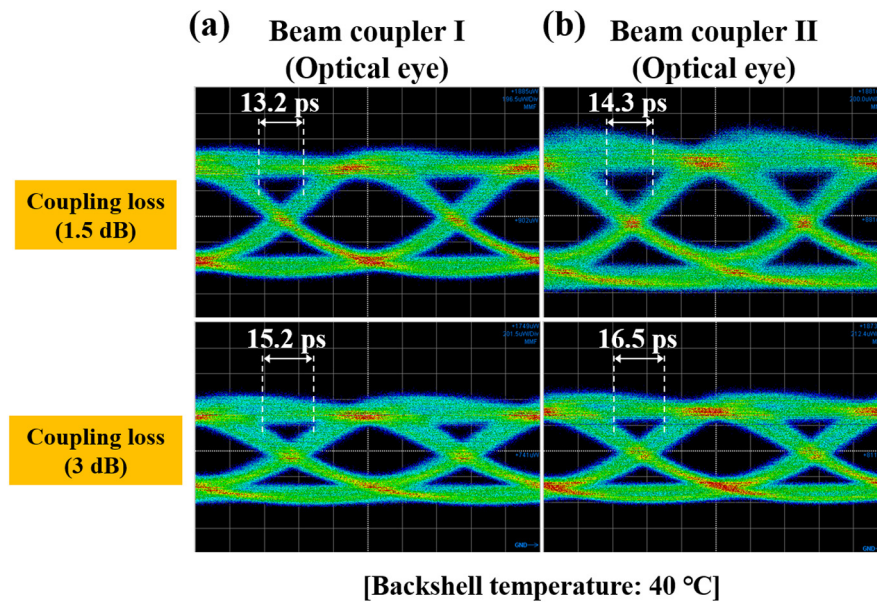


Fig. 9. Outcome of 28-Gbps data transmission for the manufactured optical engine according to the coupling loss. Output optical signals for the Tx optical engine based on (a) beam coupler I and (b) beam coupler II.

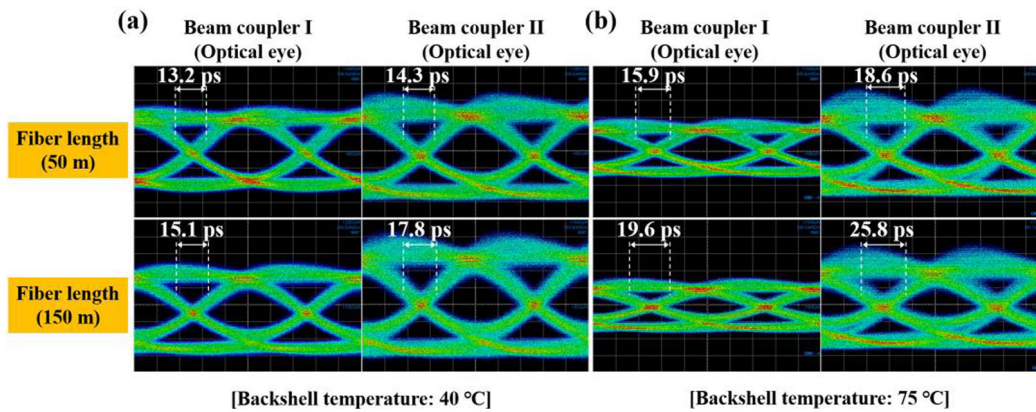


Fig. 10. Output optical eye patterns for the Tx optical engine according to the temperatures of the backshell at (a) 40 °C and (b) 75 °C.

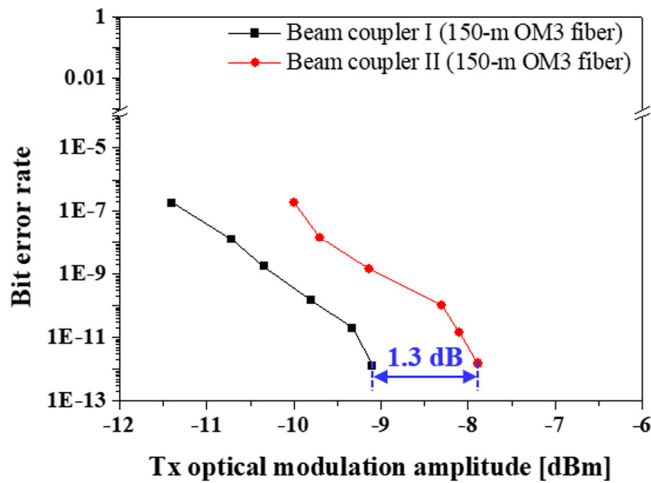


Fig. 11. Measured BER with the Tx optical modulation amplitude for a 150-m long OM3 fiber at 40 °C.

overnight at the backshell temperature of 75 °C, working as an efficient interconnect operating at 28 Gbps.

Acknowledgments

This work was partially supported by a National Research Foundation of Korea (NRF) funded by the Ministry of Education (No. 2018R1A6A1A03025242). multiLane is acknowledged for supporting the test equipment.

References

- [1] W. Xia, P. Zaho, Y. Wen, H. Xie, A survey on data center networking (DCN): Infrastructure and operations, *IEEE Commun. Surv. Tutor.* 19 (2017) 640–656.
- [2] C. Kachris, K. Kanonakis, I. Tomkos, Optical interconnection networks in data centers: Recent trends and future challenges, *IEEE Commun. Mag.* 51 (2013) 39–45.
- [3] A. Ghiasi, Large data centers interconnect bottlenecks, *Opt. Express* 23 (2015) 2085–2090.
- [4] E.K. Kang, Y.W. Lee, S. Ravindran, J.K. Lee, H.J. Choi, G.W. Ju, J.W. Min, Y.M. Song, I.B. Sohn, Y.T. Lee, 4 channel x 10 Gb/s bidirectional optical subassembly using silicon optical bench with precise passive optical alignment, *Opt. Express* 24 (2016) 10777–10785.
- [5] Z. Li, I. Shubin, X. Zhou, Optical interconnects: Recent advances and future challenges, *Opt. Express* 23 (2015) 3717–3720.

- [6] C. DeCusatis, Optical interconnect networks for data communications, *J. Lightwave Technol.* 32 (2014) 544–552.
- [7] M. Alizadeh, T. Edsall, On the data path performance of leaf-spine datacenter fabrics, in: 21st Annual Symposium on High-Performance Interconnects, IEEE, San Jose, 2013, pp. 71–74.
- [8] C. Xie, Datacenter optical interconnects: Requirements and challenges, in: Optical Interconnects Conference, IEEE, Santa Fe, 2017, pp. 37–38.
- [9] H. Li, X. Jia, Comparative study on strained InGaAs quantum wells for high-speed optical interconnect VCSELS, *Opt. Commun.* 415 (2018) 1–5.
- [10] A. Liang, C. Yang, C. Zhang, Y. Liu, F. Zhang, Z. Zhang, H. Li, Experimental study of support vector machine based nonlinear equalizer for VCSEL based optical interconnect, *Opt. Commun.* 427 (2018) 641–647.
- [11] R.A. Panicker, J.M. Kahn, Algorithms for compensation of multimode fiber dispersion using adaptive optics, *J. Lightwave Technol.* 27 (2009) 5790–5799.
- [12] K.P. Ho, J.M. Kahn, Statistics of group delays in multimode fiber with strong mode coupling, *J. Lightwave Technol.* 29 (2011) 3119–3127.
- [13] J.C. Jacob, R.K. Mishra, K. Appaiah, Quantization and feedback of principle modes for dispersion mitigation and multiplexing in multimode fibers, *IEEE Trans. Commun.* 64 (2016) 5149–5161.
- [14] M.B. Shemirani, J.M. Kahn, Compensation of multimode fiber dispersion by optimization of launched amplitude, phase, and polarization, *J. Lightwave Technol.* 28 (2010) 2084–2095.
- [15] J.A. Tatum, D. Gazula, L.A. Graham, J.K. Guenter, R.H. Johnson, J. King, C. Kocot, G.D. Landry, I. Lyubomirsky, A.N. MacInnes, E.M. Shaw, K. Balemarchy, R. Shubochkin, D. Vaidya, M. Yan, F. Tang, VCSEL-based interconnects for current and future data centers, *J. Lightwave Technol.* 33 (2015) 727–732.
- [16] D. Schoellner, S. Lutz, K. Wang, D. Kurtz, T. Kerr, M. Wang, A mechanical-optical interface for 25+ Gbps VCSEL/PD fiber coupling, in: Proc. of SPIE 10109, Optical Interconnects XVII, San Francisco, 2017, pp. 1–13.
- [17] Y.G. Lee, P. Ji, S.S. Lee, Y.S. Son, Alignment tolerant slim optical interconnect for on-board interconnections, *J. Lightwave Technol.* 34 (2016) 992–996.
- [18] H.S. Lee, S.S. Lee, B.S. Kim, Y.S. Son, Highly efficient active optical interconnect incorporating a partially chlorinated ribbon POF in conjunction with a visible VCSEL, *Opt. Express* 22 (2014) 11778–11787.
- [19] A. Mutig, J.A. Lott, S.A. Blokhin, P. Moser, P. Wolf, W. Hofmann, A.M. Nadtochiy, D. Bimberg, Modulation characteristics of high-speed and high-temperature stable 980 nm range VCSELS operating error free at 25 Gbit/s up to 85 °C, *IEEE J. Sel. Top. Quantum* 17 (2011) 1568–1575.
- [20] B.E.A. Saleh, M.C. Teich, Fundamentals of Photonics, John Wiley & Sons, Inc., 2007, Chapter 9.
- [21] O. Ziemann, J. Krauser, P.E. Zamzow, W. Daum, POF-Polymer Optical Fibers for Data Communication, Springer-Verlag Berlin Heidelberg, 2002, Chapter 1.
- [22] J.B. Schlager, M.J. Hackert, P. Pepeljugoski, J. Gwinn, Measurements for enhanced bandwidth performance over 62.5-/spl mu/m multimode fiber in short-wavelength local area networks, *J. Lightwave Technol.* 21 (2003) 1276–1285.
- [23] F.S. Tan, O. Sugihara, T. Kaino, Encircled flux-based optimized simple launch condition for standardization of multimode polymer optical waveguide evaluations, *Opt. Express* 18 (2010) 23554–23561.
- [24] P. Pepeljugoski, S.E. Golowich, A.J. Ritger, P. Kolesar, A. Risteski, Modeling and simulation of next-generation multimode fiber links, *J. Lightwave Technol.* 21 (2003) 1242–1255.